



HAL
open science

Tree-ring isotopes from *Araucaria araucana* as useful proxies for climate reconstructions

Tiphaine Penchenat, Valérie Daux, Ignacio Mundo, Monique Pierre, Michel Stievenard, Ana Srur, Laia Andreu-Hayles, Ricardo Villalba

► To cite this version:

Tiphaine Penchenat, Valérie Daux, Ignacio Mundo, Monique Pierre, Michel Stievenard, et al.. Tree-ring isotopes from *Araucaria araucana* as useful proxies for climate reconstructions. *Dendrochronologia*, 2022, 74, pp.125979. 10.1016/j.dendro.2022.125979 . hal-03702865

HAL Id: hal-03702865

<https://hal.science/hal-03702865>

Submitted on 22 Jul 2024

HAL is a multi-disciplinary open access archive for the deposit and dissemination of scientific research documents, whether they are published or not. The documents may come from teaching and research institutions in France or abroad, or from public or private research centers.

L'archive ouverte pluridisciplinaire **HAL**, est destinée au dépôt et à la diffusion de documents scientifiques de niveau recherche, publiés ou non, émanant des établissements d'enseignement et de recherche français ou étrangers, des laboratoires publics ou privés.



Distributed under a Creative Commons Attribution - NonCommercial 4.0 International License

1 **Tree-ring isotopes from *Araucaria araucana* as useful proxies for climate reconstructions**

2 Penchenat Tiphaine^{a*}, Daux Valérie^a, Mundo Ignacio^{b,c}, Pierre Monique^a, Stievenard Michel^a,

3 Srur Ana^b, Andreu-Hayles Laia^{d,e,f} and Villalba Ricardo^b

4 ^aLaboratoire des sciences du climat et de l'environnement (LSCE), Université Paris-Saclay, CNRS, CEA,
5 UVSQ, Orme de Merisiers, 91191 Gif-sur-Yvette, France

6 ^bInstituto Argentino de Nivología, Glaciología y Ciencias Ambientales (IANIGLA), CONICET, Av.
7 Ruiz Leal s/n Parque General San Martín, Mendoza, Argentina

8 ^c Facultad de Ciencias Exactas y Naturales, Universidad Nacional de Cuyo, Padre Contreras 1300,
9 Mendoza, Argentina

10 ^dTree-Ring Laboratory, Lamont-Doherty Earth Observatory of Columbia University, 61 Route 9W,
11 Palisades, NY 10964, USA

12 ^eCREAF, Bellaterra (Cerdanyola del Vall.s), Barcelona, Spain

13 ^fICREA, Pg. Llu.s Companys 23, Barcelona, Spain

14

15 *Corresponding authors:

16 Tiphaine Penchenat

17 Université Paris-Saclay, CNRS, CEA, UVSQ, Laboratoire des sciences du climat et de
18 l'environnement, Orme des Merisiers, 91191 Gif-sur-Yvette, France

19 E-mail: tiphaine.penchenat@lsce.ipsl.fr

20 Valérie Daux

21 Université Paris-Saclay, CNRS, CEA, UVSQ, Laboratoire des sciences du climat et de
22 l'environnement, Orme des Merisiers, 91191 Gif-sur-Yvette, France
23 E-mail: valerie.daux@lsce.ipsl.fr

24

25 Authors' e-mail addresses:

26 iamundo@mendoza-conicet.gob.ar

27 monique.pierre@lsce.ipsl.fr

28 michel.stievenard@lsce.ipsl.fr

29 ricardo@mendoza-conicet.gob.ar

30 asrur@mendoza-conicet.gob.ar

31 _lah@ldeo.columbia.edu

32 Abstract

33

34 Tree-ring width (TRW) chronologies have been widely and long-time used to reconstruct past climate
35 variations in the Andes in South America. The use of tree-ring isotopic chronologies is still not
36 widespread in this region although they have proved to be very efficient climate proxies. *Araucaria*
37 *araucana* (Molina) K. Koch is a conifer tree species with some multi-century-old individuals that
38 offers an excellent opportunity to measure stable carbon ($\delta^{13}\text{C}$) and oxygen ($\delta^{18}\text{O}$) isotopes in
39 cellulose from long tree-ring records. Here, we explore whether current or stored carbohydrates are
40 used for *A. araucana* radial growth and we assess the potential of a tree-ring isotopic record of to
41 study past climate variability. Eleven *A. araucana* cores from a dry and high-elevation forest at the
42 northern border of Patagonia, Argentina (38°55'S, 70°44'W) were selected for stable isotopes
43 analyses. The strong correlation between the isotopic composition of the first and second parts of

44 the same ring, but also the strong relationships between $\delta^{13}\text{C}$ and $\delta^{18}\text{O}$ records with climate
45 parameters of the current growing season such as temperature, show that tree-rings are built mostly
46 with carbohydrates produced during the current growing season with little or no supply from storage
47 or reserves. This finding leads to reconsidering the interpretation of the legacy effect (i.e. ecological
48 memory effects) based on the previously described strong negative correlation between *A. araucana*
49 TRW chronologies and previous growing season temperature and suggests a dependence of radial
50 tree growth on the level of development of organs. Regarding climate sensitivity, the *A. araucana*
51 tree-ring $\delta^{13}\text{C}$ chronology is strongly related to current summer temperature ($r = 0.82$, $p < 0.001$),
52 vapour pressure deficit (VPD; $r = 0.79$, $p < 0.001$), precipitation ($r = -0.53$, $p < 0.001$) and SPEI2 ($r = -$
53 0.73 , $p < 0.001$). These strong relationships support the use of $\delta^{13}\text{C}$ of *A. araucana* tree-ring cellulose
54 to reconstruct past temperature variations at regional scale in relation with large-atmospheric
55 drivers of climate variability such as the Southern Annular Mode. The *A. araucana* tree-ring $\delta^{18}\text{O}$
56 chronology is also correlated with temperature ($r = 0.42$, $p < 0.01$) and VPD ($r = 0.45$, $p < 0.01$) of the
57 winter preceding the growing season. This suggests that trees are using water from precipitation
58 infiltrated in the soil during the previous recharge period (autumn-winter). The weak correlations of
59 $\delta^{18}\text{O}$ with current summer atmospheric conditions and the decoupling between $\delta^{18}\text{O}$ and $\delta^{13}\text{C}$, may
60 be due to a high rate of oxygen exchange between sugars and xylem water (P_{ex}) during cellulose
61 synthesis, which dampens evaporative isotopic fractionation.

62 **Keywords:** *Araucaria araucana*, $\delta^{13}\text{C}$, $\delta^{18}\text{O}$, tree-ring width, carbohydrates
63

64 1 Introduction 65

66 Tree-rings have made an important contribution to our understanding of climatic variations over the
67 last centuries and millennia in the Andes (Boninsegna et al., 2009; Villalba et al., 2003). Climate-
68 sensitive *Polylepis tarapacana* in the Altiplano in South America provide the highest-elevation tree-
69 ring chronologies worldwide spanning for centuries to millennia (Morales et al., 2012). Even closer to

70 the Equator at 11° S, but with shorter time span, *Polylepis rodolfo-vasquezii* have also shown climate
71 sensitivity, in particular with growing season temperature (Requena-Rojas et al., 2020). Further south
72 in the Central Andes in Chile (32°S - 36°S), centennial oscillations in precipitation were inferred from
73 millennium-long records of *Austrocedrus chilensis* (Le Quesne et al., 2006, among others). Tree-ring
74 records have also provided substantial insight into regional temperature and precipitation variations
75 in northern Patagonia from recent centuries to the last millennium. Millennium-long chronologies
76 from *Fitzroya cupressoides* have been used to reconstruct past temperature variations on both sides
77 of the Northern Patagonian Andes (Lara et al., 2020, among others), while precipitation variability in
78 this region have largely been based on moisture-sensitive *Araucaria araucana* - *A. chilensis*
79 chronologies (Boninsegna et al., 2009 and references therein, Hadad et al., 2021).

80 During the past two decades, several studies have measured stable carbon and oxygen isotopic
81 composition in tree-ring cellulose ($\delta^{13}\text{C}$ and $\delta^{18}\text{O}$ respectively) from various tree species in the South
82 American Andes such as *Nothofagus pumilio* (Grießinger et al., 2018; Lavergne et al., 2017a, 2017b,
83 2016; Tognetti et al., 2014), *Nothofagus betuloides* (Meier, 2019); *A. chilensis* (Roig et al., 2006), *F.*
84 *cupressoides* (Lavergne et al., 2018, 2017a, 2016; Urrutia-Jalabert et al., 2015c); *P. tarapacana*
85 (Rodriguez-Caton et al., 2021), *A. araucana* (Arco Molina et al., 2019). These isotopic records
86 exhibited significant correlations with local climate and/or hemispheric patterns of climate variability
87 such as the Southern Annular Mode and ENSO. These strong links indicate that $\delta^{18}\text{O}$ and $\delta^{13}\text{C}$
88 chronologies are useful tools for reconstructing past climate and environmental conditions, as well as
89 past atmospheric dynamics in the South America sector of the Southern Hemisphere.

90 The carbon and oxygen data have also been used to determine if the tree-ring cellulose was
91 originated from current or stored carbohydrates (Kimak and Leuenberger, 2015; Kress et al., 2009).
92 The remobilization of stored carbohydrates is frequently observed in deciduous trees, in particular
93 during the formation of earlywood (Helle and Schleser, 2004). Although they do not generally rely on
94 reserves for initiating their growth, evergreen species can also show a strong carbon carry-over effect

95 (*Pinus kesiya* and *Pinus armandii*; Fu et al., 2017). When tree-rings are formed with both remobilized
96 stored material and current assimilates, the tree-ring cellulose $\delta^{18}\text{O}$ and $\delta^{13}\text{C}$ usually hold complex
97 and mixed information about the environmental conditions during the current growing season and
98 previous periods of carbohydrates production (Helle and Schleser, 2004; Kagawa et al., 2006).
99 Therefore, it is essential to determine the origin of the carbohydrates used for growth prior to
100 undergoing isotope-based climate reconstructions.

101 To our knowledge, only two studies conducted on *A. araucana* have included tree-ring stable iso-
102 topes as diagnostic tools. $\delta^{13}\text{C}$ was used, indeed, to estimate the evolution of intrinsic water use effi-
103 ciency (iWUE) and evaluate the physiological response of this species to climate change and the in-
104 crease in atmospheric CO_2 concentrations by Arco Molina et al. (2019). Recently, Puchi et al. (2021)
105 studied *A. araucana* stands in Northern Patagonia and showed that tree-ring isotopes and anatomi-
106 cal traits could be combined to identify stands at risk of drought-induced dieback .

107 The present study was conducted in northwestern Patagonia where trees from a dry and high-
108 elevation forest were targeted to study the use of current assimilation carbon or stored
109 carbohydrates in *A. araucana*, as well as the potential of their $\delta^{18}\text{O}$ and $\delta^{13}\text{C}$ tree-rings as climate
110 proxies. Specifically, we first determined the origin (current or prior year) of carbohydrates used for
111 tree radial growth by analyzing the influence of previous and current year conditions on the isotopic
112 signature in the cellulose and measuring intra-ring variations. Second, we compared the conclusions
113 derived from the isotopes with those drawn from the growth patterns and proposed an integrative
114 explanation for apparently incompatible findings. Finally, we debated on the strength of the climate
115 signal and the spatial representativeness of the relationships between tree-ring isotopic
116 compositions and climate parameters. Thus, we tested whether the use of C and O isotope ratios
117 could provide new climatic information in addition to that recorded by the conventional
118 dendroclimatic approach based on tree-ring widths.

119 2 Materials and Methods

120

121 *A.araucana* is an emblematic tree in the northern Patagonian forest from Argentina and Chile,
122 encompassing a latitudinal three-degree range from 37°20'S to 40°20'S approximately (Veblen et al.,
123 1995). In Argentina, *A. araucana* is confined along the Andes mountains between 38°40'S and
124 39°20'S in the province of Neuquén. *A. araucana* is adapted to highly contrasting environments
125 growing from very humid (4000 mm/year at some Chilean sites) to dry environments (e.g. ~500
126 mm/year) (Veblen, 1982; Veblen et al., 1995). It forms monospecific stands, but it is often associated
127 with *Nothofagus antarctica* and *N. pumilio*, mostly on south-facing slopes at elevations between
128 1000 and 1400 m a.s.l. (Veblen et al., 1995). Mixed stands with *A. chilensis*, *Lomatia hirsuta* and
129 other shrub species are recorded at ecotonal environments with the Patagonian steppe in the
130 eastern distribution sector (Burns, 1991, 1993).

131

132 2.1. Tree species and study site

133

134 Trees from *A. araucana* were sampled at Sainuco, a site located in a dry and high-elevation location
135 for the species, and supposedly sensitive area in the northwestern of Patagonia. The Sainuco
136 sampling site (SAI, 38°55'S, 70°44'W) is located at 1660 m a.s.l elevation on a southeast-facing slope
137 at the northern portion of the Sierra de Catán Lil, 57 km east of the main Andes divide (Fig. 1a). The
138 soil is from the Andisol order (del Valle, 1998). At Sainuco, *A. araucana* forms a monospecific, open
139 stand (Fig. 1b), mostly composed by mature individuals with a density of about 100 trees per hectare.
140 The lack of young trees is likely due to cattle feeding on fallen seeds (Burns, 1991). The annual mean
141 temperature and total precipitation at Sainuco are 8.4 ± 0.4 °C and 516 ± 94 mm, respectively, over
142 the period 1974-2014 (See Meteorological data section; CRU TS 4.3 database, Harris et al., 2020).
143 Regarding climate seasonality, lower temperatures occurred from May to August when most of the
144 precipitation is received (Fig. 1c).

145

146 2.2 Sample collection and preparation

147

148 Cores from *A. araucana* at the Sainuco site were taken in November 2015 and processed at the
149 Instituto Argentino de Nivología, Glaciología y Ciencias Ambientales (IANIGLA CONICET), Mendoza,
150 Argentina. Initially used for ring width dendrochronological analyses, cores were mounted and
151 sanded following Stokes and Smiley (1968), visually crossdated using the Yamaguchi (1991) approach.
152 Ring widths were measured to the nearest 0.001 mm, and the computer program COFECHA (Holmes,
153 1983) was used to detect measurement and dating errors. The individual tree-ring width timeseries
154 were computed to generate a regional *A. araucana* ring width chronology (Mundo et al., 2012).
155 Regarding the calendar dating, as in the Southern Hemisphere the growing season straddles two
156 calendar years each annual ring was assigned to the year in which ring formation started following
157 the Schulman's convention (1956). The transition from the previous to the current biological year
158 takes place between April and September, i.e. mid fall to early spring.

159 The oldest 10 trees, with ages ranging between 240 and 546 years old were selected for the isotopic
160 analyses. At the Laboratoire des Sciences du Climat et de l'Environnement (LSCE, Gif-sur-Yvette,
161 France), the mounted cores were peeled off using hot water and dried for several hours at ambient
162 air. For each core, forty-one annual rings (1974 - 2014) were split using a scalpel, and the α -cellulose
163 was extracted from the wood of each ring sample following the chemical procedure described by
164 Leavitt and Danzer (1993). In order to quantify the intra-ring variability of the isotopic compositions
165 of oxygen and carbon, an additional core (named 'intra-core' hereafter) with wide rings was selected
166 and earlywood and latewood were cut and analyzed separately over the 1950-2014 period. Since the
167 transition from earlywood to latewood in *A. araucana* tree-rings is very gradual and consequently
168 difficult to situate unambiguously, we divided the rings into two parts: the first portion
169 corresponding to the first three quarters of the ring (F3/4) and the second portion to the last fourth
170 (L1/4), as shown in figure 2. Therefore, the wood did not strictly correspond to early- and latewood

171 but nevertheless reflected successive phases during the growth period. These parts were weighted,
172 processed and analyzed in the same way as the complete rings of the other 10 samples. The L1/4
173 sample of 1998 was lost during cellulose extraction due to very small amount of wood.

174

175 2.3 Measurement of carbon and oxygen isotopes in tree-rings

176

177 The isotopic compositions of oxygen and carbon of tree-ring cellulose were simultaneously obtained
178 by high temperature pyrolysis (HTP) in a high temperature conversion elemental analyzer (TC-EA,
179 Thermo Scientific) coupled to a mass spectrometer (IRMS, IsoPrime). To correct for potential
180 instrumental drifts, a cellulose standard (Whatmann © CC31) was analysed every three samples in
181 each sequence of analysis. The analytical precisions of the instrument were within 0.20 ‰ and 0.10
182 ‰ for oxygen and carbon, respectively, based on the standard uncertainty of the mean. HTP was
183 shown to be a suitable and reliable proceeding for the determination of the isotopic composition of
184 carbon in cellulose simultaneously during the analysis of oxygen ratios. Although an isotope effect
185 related to the non-statistical conversion of the organic carbon to CO may alter the results for carbon
186 (Knöller et al., 2005), we prevented this issue by adjusting the results from the HTP using a
187 combustion-pyrolysis regression previously obtained with pairs of measurements as proposed in
188 Woodley et al. (2012). Therefore, the adjusted carbon values were equivalent to the values that
189 would have been obtained using combustion.

190 The oxygen and carbon isotopic compositions were expressed as δ ($\delta^{13}\text{C}$ for carbon and $\delta^{18}\text{O}$ for
191 oxygen), in per mill (‰):

$$192 \quad \delta = (R_{\text{cell}}/R_{\text{STD}} - 1) \times 1000 \quad (1)$$

193 where R_{cell} is the oxygen isotope ratio ($^{18}\text{O}/^{16}\text{O}$) of cellulose referring to R_{STD} , the Vienna Standard
194 Mean Ocean Water (Coplen, 1996), or the carbon isotope ratio ($^{13}\text{C}/^{12}\text{C}$) of cellulose referring to R_{STD} ,
195 the Vienna Pee-Dee Belemnite (Coplen, 1996).

196 The $\delta^{13}\text{C}$ records show a decreasing trend over time due to the decrease in $\delta^{13}\text{C}$ of atmospheric CO_2
197 since the beginning of industrialization. Therefore, the measured $\delta^{13}\text{C}$ were corrected for this
198 anthropogenic isotopic effect using the standard $\delta^{13}\text{C}$ correction model from Dombrosky (2020).
199 Hereafter, the physiological and (paleo-)climatic interpretations were made on the basis of these
200 corrected $\delta^{13}\text{C}$ values.

201

202 2.4 Chronology development

203

204 The individual $\delta^{18}\text{O}$ and $\delta^{13}\text{C}$ series were averaged to generate isotopic site chronologies, hereafter
205 $\delta^{18}\text{O}_{\text{SAI}}$ and $\delta^{13}\text{C}_{\text{SAI}}$ chronologies (data in Supplementary Material).

206 Several descriptive statistics were calculated to assess the coherence between individual series and
207 the final quality of the chronologies: r (Pearson correlation coefficient), CI (Confidence Intervals),
208 RBAR (mean Pearson correlation coefficient among tree-ring series within a chronology; Briffa, 1995)
209 and EPS (Expressed Population Signals; Wigley et al., 1984). EPS enables to assess how well a mean
210 chronology based on a finite number of series represents the hypothetical perfect chronology
211 consisting of an infinite number of series (Wigley et al., 1984). CI was calculated for each year
212 according to the following equation:

$$213 \quad \text{CI} = t \times (\text{SD}/\sqrt{N}) \quad (2)$$

214 Where SD is the standard deviation, N is the number of individual series and t is the two-tailed
215 Students' t value at 95 % confidence.

216

217 2.5 Meteorological data

218

219 We used the climate data (1973 and 2015) from the two nearest grid points to our sampling site
220 taken from CRU TS 4.3 gridded database (70.75°W - 38.75°S and 70.75°W - 39.25°S; Harris et al.,
221 2020; <https://crudata.uea.ac.uk/cru/data/hrg/>). From these gridded points regional monthly
222 maximum and minimum temperatures (T_{\max} , T_{\min} in °C), precipitation (PRE, in mm) and actual vapour
223 pressure (AVP, in hPa) were retrieved. The monthly vapour pressure deficit (VPD_{\max}) was calculated
224 as the difference between the monthly saturated vapour pressure (SVP_{\max}) and the AVP. SVP_{\max} was
225 calculated with the Tetten (1930)'s equation:

$$226 \quad SVP = 6.108 \times \exp(17.27 \times T / 237.3 + T) \quad (3)$$

227 Where T is T_{\max} in Celsius degree, and SVP is in kPa.

228 VPD_{mean} was calculated using SVP_{mean} (average of SVP_{\max} and SVP_{\min}). Its variations are very similar to
229 those of VPD_{\max} (correlation coefficient of 0.97). For coherency with T_{\max} , VPD_{\max} is used and
230 discussed in this paper.

231 We also extracted the Standardized Precipitation-Evapotranspiration Index (SPEI), to compare our
232 results with a drought index (Vicente-Serrano et al., 2010; <https://spei.csic.es/>), and the monthly
233 photosynthetically active radiation flux (PAR, in W/m^2) from the NASA/GEWEX Surface Radiation
234 Budget Release 3.0 dataset (<https://asdc.larc.nasa.gov/project/SRB>). We present in this paper the
235 most significant results which were obtained with SPEI calculated on a two-month timescale (SPEI2).
236 From ERA5 (ECMWF's fifth generation atmospheric global climate reanalysis covering the period
237 January 1950 to the present; Hersbach et al., 2020;
238 [https://cds.climate.copernicus.eu/cdsapp#!/dataset/reanalysis-era5-single-levels-monthly-](https://cds.climate.copernicus.eu/cdsapp#!/dataset/reanalysis-era5-single-levels-monthly-means?tab=form)
239 [means?tab=form](https://cds.climate.copernicus.eu/cdsapp#!/dataset/reanalysis-era5-single-levels-monthly-means?tab=form)), we extracted atmospheric maximum temperature at 2 meters above ground level
240 ($T2m$, in K) and surface pressure 850 mb (SLP, in Pa). We also used the Southern Annular Mode
241 (SAM) index from ERA5 (difference between $slp40$ and $slp65$) because the SAM is the main mode of
242 climate variability at high latitudes in the Southern Hemisphere (Garreaud et al., 2013).

243 Spatial correlation patterns between the Sainuco isotopic chronologies and T_{max} , SPEI2, PRE, T2m and
244 SLP 850 mb were obtained for the interval 1974-2014 using the KNMI Climate Explorer web
245 application (<https://climexp.knmi.nl/>).

246

247 3 Results

248

249 The RBAR and EPS values for the $\delta^{13}C$ series were 0.22 and 0.74, respectively. For the $\delta^{18}O$ series,
250 these statistics were equal to 0.54 and 0.92, which shows a greater shared variance among the $\delta^{18}O$
251 individual series (Fig. 3). For 10 trees, the CI were 0.49 ‰ and 0.66 ‰ for $\delta^{13}C_{SAI}$ chronology and
252 $\delta^{18}O_{SAI}$ chronology respectively. Over 1974-2014, for the $\delta^{13}C_{SAI}$ and $\delta^{18}O_{SAI}$ chronologies, the average
253 and standard deviations (SD) were -20.09 ± 0.69 ‰ and 30.44 ± 0.94 ‰, respectively, and the trends
254 were both positive ($+0.002$ and $+0.015$ ‰), but not significant at 95 % confidence level. The one-lag
255 autocorrelation coefficients were 0.20 (non-significant (ns), $n = 41$) and 0.31 ($p < 0.05$, $n = 41$) for
256 carbon and oxygen respectively, indicating that $\delta^{18}O_{SAI}$ was slightly more affected by past
257 physiological and/or environmental conditions than $\delta^{13}C_{SAI}$. The $\delta^{13}C_{SAI}$ and $\delta^{18}O_{SAI}$ chronologies were
258 not significantly correlated to one another ($r = -0.23$, ns, $n = 41$).

259 Over 1950-2014, the $\delta^{13}C$ chronologies obtained for F3/4 ($\delta^{13}C_{F3/4}$) and L1/4 ($\delta^{13}C_{L1/4}$) showed slightly
260 positive, but non-significant trends (Fig. 4), and were positively and strongly correlated with each
261 other ($r = 0.71$, $p < 0.001$, $n = 64$; Fig. 5). The correlation coefficient between $\delta^{13}C_{SAI}$ and $\delta^{13}C_{F3/4}$ ($r =$
262 0.51 , $p < 0.001$, $n = 41$) was larger than between $\delta^{13}C_{SAI}$ and $\delta^{13}C_{L1/4}$ ($r = 0.46$, $p < 0.01$, $n = 40$). The
263 isotopic composition of the whole rings, hereafter $\delta^{13}C_{WR}$, was calculated as the sum of $\delta^{13}C_{F3/4}$ and
264 $\delta^{13}C_{L1/4}$, weighted by the mass of cellulose chemically extracted from the F3/4 and L1/4. The
265 correlation coefficient between $\delta^{13}C_{WR}$ and $\delta^{13}C_{SAI}$ was 0.52 ($p < 0.001$, $n = 40$), which equals the
266 mean value of the correlation coefficients between the individual $\delta^{13}C$ series and $\delta^{13}C_{SAI}$.

267 The two $\delta^{18}\text{O}$ series obtained for F3/4 ($\delta^{18}\text{O}_{\text{F3/4}}$) and L1/4 ($\delta^{18}\text{O}_{\text{L1/4}}$) showed also slightly positive
268 trends, but not-significant (Fig. 4). The correlation between $\delta^{18}\text{O}_{\text{F3/4}}$ and $\delta^{18}\text{O}_{\text{L1/4}}$ was the same as the
269 one between $\delta^{13}\text{C}_{\text{F3/4}}$ and $\delta^{13}\text{C}_{\text{L1/4}}$ ($r = 0.70$, $p < 0.001$, $n = 64$). The correlation between $\delta^{18}\text{O}_{\text{SAI}}$ and
270 $\delta^{18}\text{O}_{\text{F3/4}}$ ($r = 0.68$, $p < 0.001$, $n = 41$) was similar to the correlation between $\delta^{18}\text{O}_{\text{SAI}}$ and $\delta^{18}\text{O}_{\text{L1/4}}$ ($r =$
271 0.65 , $p < 0.001$, $n = 40$; Fig. 5). The isotopic composition of the whole rings, hereafter $\delta^{18}\text{O}_{\text{WR}}$, was
272 calculated as the sum of $\delta^{18}\text{O}_{\text{F3/4}}$ and $\delta^{18}\text{O}_{\text{L1/4}}$, weighted by the mass of cellulose chemically extracted
273 from the F3/4 and L1/4. The correlation coefficient obtained between $\delta^{18}\text{O}_{\text{WR}}$ and $\delta^{18}\text{O}_{\text{SAI}}$ was 0.71 (p
274 < 0.001 , $n = 40$). Interannual variations in the $\delta^{13}\text{C}$ and $\delta^{18}\text{O}$ of F3/4 and L1/4 were consistent with
275 those of the average Sainuco chronologies (Fig. 4).

276 The correlation coefficient of current year $\delta^{13}\text{C}_{\text{F3/4}}$ with current year $\delta^{13}\text{C}_{\text{L1/4}}$ ($r = 0.71$, $p < 0.001$, $n =$
277 64) was higher than with previous year $\delta^{13}\text{C}_{\text{L1/4}}$ ($r = 0.34$, $p < 0.01$, $n = 64$, Fig. 5). Similarly, the
278 correlation of current year $\delta^{18}\text{O}_{\text{F3/4}}$ with current year $\delta^{18}\text{O}_{\text{L1/4}}$ ($r = 0.70$, $p < 0.001$, $n = 64$) was higher
279 than with previous year $\delta^{18}\text{O}_{\text{L1/4}}$ ($r = 0.51$, $p < 0.001$, $n = 64$).

280 Using linear regressions, we assessed trends in T_{max} , VPD_{max} , SPEI2 and PRE from 1974 to 2014. We
281 found an increasing trend in T_{max} particularly during December-January ($+0.9^\circ\text{C}$, i.e. around $+0.2^\circ\text{C}$
282 per decade) and VPD_{max} ($+1.2$ hPa, i.e. $+0.3$ hPa per decade) for the same period, and consistent
283 decreasing ones in SPEI2 and PRE (-60 mm in annual average, i.e. -15 mm per decade) (Fig. 1d).

284 Correlation analyses were performed between $\delta^{13}\text{C}_{\text{SAI}}$ and $\delta^{18}\text{O}_{\text{SAI}}$ and the climate data. The monthly
285 correlations of $\delta^{13}\text{C}_{\text{SAI}}$ and $\delta^{18}\text{O}_{\text{SAI}}$ with T_{max} , VPD_{max} , SPEI2 and PRE are shown in figure 6. The most
286 significant relationship between $\delta^{13}\text{C}_{\text{SAI}}$ and climate was with December-January T_{max} of the current
287 growing season ($r = 0.82$, $p < 0.001$, $n = 41$; Fig. 7). There was also a significant positive correlation
288 between $\delta^{13}\text{C}_{\text{SAI}}$ and VPD_{max} over the same period ($r = 0.79$, $p < 0.001$, $n = 41$; Fig. 7), consistently with
289 the fact that T_{max} is involved in the calculation of VPD_{max} . We also recorded a significant negative
290 correlation between $\delta^{13}\text{C}_{\text{SAI}}$ and January SPEI2 (i.e. calculated over December-January) during the
291 current growing season ($r = -0.73$, $p < 0.001$, $n = 41$; Fig. 7). A negative correlation was evidenced

292 between $\delta^{13}\text{C}_{\text{SAI}}$ and December PRE of the current growing season ($r = -0.53$, $p < 0.001$, $n = 41$). A
293 positive correlation was found between $\delta^{13}\text{C}_{\text{SAI}}$ and SAM in November-December of the current
294 growing season ($r = 0.39$, $p < 0.05$, $n = 41$). $\delta^{18}\text{O}_{\text{SAI}}$ did not show significant relationships with any
295 monthly meteorological data from current or previous growing seasons. In contrast, it was positively
296 related to T_{max} (May-June; $r = 0.42$, $p < 0.01$, $n = 41$) and VPD_{max} (June-August; $r = 0.45$, $p < 0.01$, $n =$
297 41) of autumn-winter of the preceding growing season.

298 Spatial correlation analyses were conducted between the $\delta^{13}\text{C}_{\text{SAI}}$ and the mean December-January
299 T_{max} (Fig. 8a), January SPEI2 (Fig. 8b) and December PRE (Fig. 8c) across the region from 30°S to 57°S
300 and from 78°W to 60°W. Significant correlations were observed over a large area in the southern
301 South America, positive with T_{max} and negative with SPEI2 and PRE. This is consistent with previous
302 results based on monthly correlations (see above). At a larger scale from 20°N – 80°S and from 160°E
303 – 30°W, December-January T2m from the ERA5 reanalyses (Fig. 8d) was also significantly correlated
304 with the $\delta^{13}\text{C}_{\text{SAI}}$ record and positively over the Southern tip of the South American continent and in
305 the Pacific around 80°W, and negatively between 50°S and 60°S in the Pacific around 120°W and on
306 the West Antarctic coasts (Bellingshausen and Amundsen seas). The spatial correlation between
307 $\delta^{13}\text{C}_{\text{SAI}}$ and December SLP exhibits a similar pattern in December (Fig. 8e).

308

309 4 Discussion

310

311 4.1 Which carbohydrates is the cellulose of *A. araucana* rings built with?

312

313 In *A. araucana*, latewood represents about 10-22 % of the ring (Falcon-Lang, 2000), but the transition
314 between early and latewood is gradual (Díaz-Vaz, 1984; Tortorelli, 1956) and the precise separation
315 of the two tissues is problematic. Therefore, in order to determine the intra-annual isotopic
316 signature, the cutting at the third fourth of each ring, in order to generate F3/4 and L1/4 series

317 approximately informs about the earlywood and latewood sections, respectively. The strong link
318 between the isotopic records of the first and second parts of the rings ($r = 0.7$ for both $\delta^{13}\text{C}$ and $\delta^{18}\text{O}$)
319 suggests that the two portions were formed from sugars synthesized in the same growing season.
320 Due to the thinness of the rings, this intra-core experiment was conducted on one core only (having
321 above average wide rings). The conclusion drawn above must therefore be taken with caution and
322 should be ideally supported by similar tests on other trees. However, the significant correlations
323 between $\delta^{13}\text{C}_{\text{F3/4}}$, $\delta^{13}\text{C}_{\text{F1/4}}$, $\delta^{13}\text{C}_{\text{WR}}$ ($\delta^{18}\text{O}_{\text{F3/4}}$, $\delta^{18}\text{O}_{\text{F1/4}}$, $\delta^{18}\text{O}_{\text{WR}}$) with the $\delta^{13}\text{C}_{\text{SAI}}$ ($\delta^{18}\text{O}_{\text{SAI}}$) demonstrate that
324 the core selected for intra-annual analyses exhibited an intra-ring isotopic pattern very likely shared
325 by the other trees of the same stand.

326 The positive relationships between $\delta^{13}\text{C}_{\text{SAI}}$ and climate parameters of the current growing season also
327 suggest that the *A. araucana* tree-rings in the Sainuco site are mostly formed with current
328 carbohydrates with little use of the previous year reserves for early season wood formation.
329 Evergreen trees can form xylem cells in early spring using carbohydrates produced by 'old' needles
330 grown in previous years, and from old and new needles afterwards (Barbour et al., 2002; Dickmann
331 and Kozłowski, 1970; Glerum, 1980; Rathgeber, 2020). They are less dependent on their reserves to
332 start their growth than deciduous species and therefore less likely to use them (Kozłowski, 1992). The
333 evidence presented above indicates that *A. araucana* trees from Sainuco likely do not rely on stored
334 carbohydrates for the onset of the growing season. They thus fit the pattern most commonly
335 observed among evergreen trees. Note that these findings cannot be extrapolated to all *A. araucana*
336 populations. Indeed, as already stressed, the intra-ring results being obtained on one single tree
337 cannot be generalised. In addition, in a general way, the photosynthates (current or stored) selected
338 for early growth may not only depend on the species, but also on the environment. The influence of
339 environmental conditions can be illustrated with a study of two populations of *F. cupressoides*
340 growing on both sides of the Andes. Different possible use of reserves in the two populations were
341 pointed out based on significant correlations between $\delta^{13}\text{C}_{\text{SAI}}$ and previous and current summer
342 temperature in the Chilean wet stands (Urrutia-Jalabert et al., 2015c), while only current summer

343 temperature was significant in the Argentinian drier sites (Lavergne et al., 2017a). More studies are
344 needed to elucidate if the humidity site conditions can be the most important factor determining the
345 use of carbohydrates during the current or previous year.

346 Importantly, as tree-ring cellulose seems to be mostly formed with current photosynthates, the
347 isotopic signal, which thus represents essentially the environmental conditions of the current
348 growing season, can be extracted without the need for conducting intra-annual cuts in the tree-ring
349 samples.

350

351 4.2 Does the functioning of *A. araucana* based on isotopic chronologies 352 agree with that derived from tree-ring widths?

353

354 The regional tree-ring width (TRW) reference chronology for the Argentinean network of *A. araucana*
355 sites (Mundo et al., 2012) is negatively correlated with summer temperature from the previous
356 growing season (TRW versus T_{DJF} : $r = -0.50$, $p < 0.001$, $n = 41$), and to a lesser extent, with the current
357 season temperature ($r = -0.32$, $p < 0.05$, $n = 41$). These dependencies are consistent with the
358 inverse and one-year lagged relationships between the TRW of *A. araucana* and summer
359 temperatures evidenced in several Patagonian sites (Hadad et al., 2014; Hadad and Roig, 2016;
360 Muñoz et al., 2013; Villalba, 1995), a pattern which emerges with most of the gymnosperms in
361 Northern Patagonia (Lara et al., 2020; Lavergne, 2016; Villalba, 1990; Villalba et al., 1998, 1996).

362 In terms of growth, the performance of trees may depend, at least partially, on reserves made the
363 previous years. It may also rely on structures from the past (needles, buds, roots, sapwood) which
364 may be several-year old and carry some information on conditions of the periods when they were
365 built (Zweifel and Sterck, 2018). Indeed, as described hereafter, these past structures may be the
366 sites where hormones essential for xylem cell formation are produced (Buttò et al., 2020).

367 Xylogenesis can be divided into several steps, including cell enlargement, which is the most

368 important for radial growth. This step is regulated by phytohormones (notably auxin indole-3-acetic
369 acid; IAA; Taiz and Zeiger, 2002), produced in the primordia and young developing leaves, roots or
370 seeds (Brumos et al., 2018; Davies, 2010; Ljung et al., 2005; Zhao, 2010). The limitation of the
371 formation of young developing leaves and fine roots leads to a weaker hormone production whose
372 action is necessary for radial growth (Dünser and Kleine-Vehn, 2015; Majda and Robert, 2018;
373 Scheuring et al., 2016). This internal regulation may explain the correlation between TRW and the
374 climatic conditions of the previous year that affect hormone production sites. As osmotic pressure is
375 the driving force behind cell enlargement (Cuny and Rathgeber, 2014), the rate of increase in cell size
376 depends on the water status of the tree, which is itself determined by the physical conditions of the
377 air and soil. The correlations between TRW and the climatic conditions of the current year (Mundo et
378 al., 2012) likely reflect this dependence.

379 Our results show that TRW, proxy of xylogenesis, and $\delta^{13}\text{C}_{\text{SAI}}$, proxy of assimilations (see Rodriguez-
380 Caton et al., 2021), are controlled by different climate conditions. While the regional TRW chronology
381 shows that the radial growth is controlled mainly by the previous summer temperature, the $\delta^{13}\text{C}_{\text{SAI}}$
382 indicates that the cellulose is mostly derived from current carbohydrates with very limited or even no
383 use of reserves. These two facts can be reconciled if we consider that the legacy effect, which
384 induces a lagged-correlation between TRW and temperature, is not due to the direct use of reserves
385 for growth, but linked to the development of organs formed in the past, controlling the production of
386 IAA growth hormone (Buttò et al., 2020). The correlation of $\delta^{13}\text{C}$ with current conditions reflects the
387 fact that the majority of biomass, including cellulose, is contained in secondary cell walls formed
388 during the second step of xylogenesis (Rathgeber et al., 2016; Zhong and Ye, 2009), very likely with
389 current year carbohydrates in the case of *A. araucana*.

390 Both the regional TRW and the $\delta^{13}\text{C}_{\text{SAI}}$ records are good proxies for temperature reconstruction but
391 the correlation between $\delta^{13}\text{C}_{\text{SAI}}$ and the meteorological parameter is the strongest (-0.5 versus 0.8 for
392 temperature), possibly because of the absence of legacy effects on the carbon signature. A stronger

393 relation with climate over the calibration period (1974-2014) likely leads to more accurate
394 reconstructions by application of the transfer functions (i.e. equations linking $\delta^{13}\text{C}_{\text{SAI}}$ with climate
395 signals, Appendix A). This advantage favors the use of $\delta^{13}\text{C}_{\text{SAI}}$ over TRW for reconstructing past
396 temperature or other strongly related parameters like VPD_{max} .

397

398 4.3 Why are the C and O isotopic compositions in *A. araucana* tree-rings 399 related to climate?

400

401 Consistently with rings formed with current season photosynthates, the $\delta^{13}\text{C}_{\text{SAI}}$ and $\delta^{18}\text{O}_{\text{SAI}}$ are
402 strongly related to several climate parameters along the current year. In the following lines we
403 develop the possible physiological mechanism behind these patterns.

404 The strong relationship between $\delta^{13}\text{C}_{\text{SAI}}$ and current summer VPD_{max} (December-January, $r = 0.79$) is
405 likely due to the control of stomatal conductance at the leaf level by VPD_{max} . Indeed, trees adjust the
406 opening of their stomata according to VPD_{max} and try to avoid as much as possible critical water
407 tension in their xylem network (Running, 1976). Stomatal conductance not only regulates water loss
408 but also the flux of CO_2 from the outside air to the substomatal cavity. Therefore, together with the
409 activity of the Rubisco enzyme, stomatal conductance controls CO_2 concentration in the substomatal
410 cavity, which in turn, controls carbon discrimination in C3 plants. The larger the VPD_{max} , the lower the
411 CO_2 substomatal concentration and the carbon isotope discrimination. The VPD_{max} influence may also
412 work through the evaporation of water from the surficial layers of the soil, affecting tree water status
413 and, thus, stomatal conductance (Grossiord et al., 2020).

414 The $\delta^{13}\text{C}_{\text{SAI}}$ is also strongly related to the summer T_{max} (December-January, $r = 0.82$). The temperature
415 signal in $\delta^{13}\text{C}_{\text{SAI}}$ may reflect the influence of temperature on VPD_{max} and in turn, of this variable on
416 stomatal conductance. Indeed, as expressed in equation 3, SVP increases exponentially with
417 temperature. As AVP does not generally increase at the same rate as temperature, warmer

418 conditions induce increased VPD_{max} , and decreased carbon isotope discrimination. The discrimination
419 is also affected by the activity of the Rubisco enzyme. The more active the enzyme, the greater the
420 carbon removal from the sub-stomatal cavity and the lower the isotopic discrimination. In C3 plants,
421 the rate of photosynthesis does not depend much on temperature under current atmospheric
422 conditions (Berry and Bjorkman, 1980). However, the catalytic activity of Rubisco decreases
423 (increases) under conditions of low (high) light intensity (Mott and Woodrow, 2000). PAR correlates
424 positively with summer T_{max} (December-January, $r = 0.55$, $p < 0.01$, $n = 25$; not shown). Thus, the
425 $\delta^{13}C_{SAI}$ -temperature link may be reinforced by the light-regulated activity of Rubisco. The dependence
426 of $\delta^{13}C_{SAI}$ on temperature reflects a chain of causality rather than a direct effect of temperature on
427 stomatal conductance and Rubisco activity.

428 The negative relations of $\delta^{13}C_{SAI}$ with PRE (December, $r = -0.53$) and SPEI2 (January, $r = -0.73$) during
429 the growing season may be indirect and result from the dependence of these meteorological
430 parameters on air saturation with water. Indeed, the higher the VPD_{max} , the less likely is water
431 condensation and therefore precipitation, but the higher is SPEI2 ($r = 0.80$, $p < 0.001$, $n = 41$ between
432 PRE and SPEI2 in December-January). $\delta^{13}C_{SAI}$ may also be related to summer PRE through the effect of
433 soil water content on stomatal conductance. However, the low December PRE is unlikely to
434 contribute significantly to soil moisture, and the relationship between PRE (from December or yearly)
435 and soil moisture can be complex. Only soil moisture monitoring could help clarifying the relation
436 between $\delta^{13}C_{SAI}$ and PRE.

437 The $\delta^{18}O_{SAI}$ is positively correlated with T_{max} (May-June, $r = 0.42$) and VPD_{max} (June-August, $r = 0.45$) of
438 the late autumn and winter before the growing season. The $\delta^{18}O$ in soil water, which trees tap from,
439 depends on the history of the air masses that provide moisture, including rainout driven by
440 temperature variations, and evaporation at soil level (Sprenger et al., 2016). The pumping of water
441 occurs without isotopic fractionation (Bariac et al., 1990; Dawson and Ehleringer, 1993; Rothfuss and
442 Javaux, 2017). At the leaf level, evaporative fractionation, a temperature-dependent process, induces

443 the isotopic enrichment of leaf water and the subsequent sugars (Cernusak et al., 2016; Gonfiantini
444 et al., 1965). Although exchanges between organic oxygen and xylem water oxygen occur during
445 cellulose synthesis, the isotopic composition of cellulose, which derives from that of sugars, also
446 presents an enriched character (e.g. Barbour and Farquhar, 2004). Thus, the relation of $\delta^{18}\text{O}_{\text{SAI}}$ with
447 T_{max} reflects the role of temperature in rainout history and/or in evaporative fractionation. The fact
448 that the highest relation between $\delta^{18}\text{O}_{\text{SAI}}$ and temperature was found during the austral winter
449 before the growing season suggests that the $\delta^{18}\text{O}_{\text{SAI}}$ likely depends more on the winter $\delta^{18}\text{O}_{\text{precipitation}}$
450 than on summer evaporative fractionation. The dependence on winter $\delta^{18}\text{O}_{\text{precipitation}}$ makes sense as
451 winter is the rainy season and very probably the water recharge period in the soil. The link between
452 $\delta^{18}\text{O}_{\text{F3/4}}$ and the previous-year $\delta^{18}\text{O}_{\text{L1/4}}$, the significant autocorrelation at 1-year lag of $\delta^{18}\text{O}_{\text{SAI}}$ ($r = 0.31$,
453 $p < 0.05$), and the dependence of $\delta^{18}\text{O}_{\text{SAI}}$ on climate parameters of the autumn-winter preceding the
454 growing season, do not contradict the conclusion drawn with $\delta^{13}\text{C}_{\text{SAI}}$ on the use for growth of the
455 current sugars. Indeed, in seasonally dry environments like Sainuco, trees may rely largely on tightly
456 bound pore water infiltrated during the previous recharge period (autumn-winter) for their water
457 supply during the dry growing season (Brooks et al., 2009). Unfortunately, there are no $\delta^{18}\text{O}_{\text{precipitation}}$
458 records long enough available in the region to be compared with our $\delta^{18}\text{O}_{\text{SAI}}$ data.

459 In dry environments, trees tend to close their stomata to avoid losing water excessively and being at
460 risk of embolism. The low $\delta^{18}\text{O}$ sensitivity to summer VPD observed at Sainuco could thus reflect a
461 strong reduction of stomatal conductance in response to low soil moisture. However, this conclusion
462 is not in agreement with the results obtained with carbon which are not in favor of stomatal closure
463 but rather of a modulation of the stomatal conductance (by VPD). Cheesman and Cernusak (2016)
464 compared leaf and trunk $\delta^{18}\text{O}_{\text{cellulose}}$ in trees along an aridity gradient. They found that leaf $\delta^{18}\text{O}_{\text{cellulose}}$
465 demonstrated a strong climatic signal all along the gradient whereas trunk $\delta^{18}\text{O}_{\text{cellulose}}$ was not
466 influenced by summer variables at dry sites. They explained the decoupling between leaf and trunk
467 isotopic composition by an increase, with decreasing humidity, of the rate of oxygen exchange

468 between sugars and xylem water (P_{ex}) during cellulose synthesis. Szejner et al. (2020) also evidenced
469 experimentally an enhancement of the proportion of the oxygen exchanged between sugars and
470 source water with decreasing relative humidity. At the dry Sainuco site, the lack of significant
471 relations between current climate variables and $\delta^{18}O_{SAI}$ may be ascribed to a high P_{ex} reinforcing the
472 source signal and dampening the climate signal.

473 The combined analysis of carbon and oxygen isotope compositions can be used to clarify the
474 interpretation of carbon discrimination assuming that a positive correlation between the two ratios
475 reflect a regulation of $\delta^{13}C_{SAI}$ by stomatal conductance rather than rubisco activity (Roden and
476 Farquhar, 2012; Scheidegger et al., 2000). However, this dual-isotope approach is fully valid if the
477 $\delta^{18}O$ of the source water of the trees is constant. As the variations of $\delta^{18}O_{SAI}$ here seem to mirror
478 those of the source, possibly because P_{ex} has a high value, the dual-isotope approach is not
479 applicable.

480 The $\delta^{13}C_{SAI}$ captured variations in summer temperature, precipitation and SPEI2 over a large area of
481 Patagonia, south of $\approx 33^\circ S$ (Fig. 8a, b and c). Yet, these different climate parameters are mainly
482 influenced by the SAM (Garreaud et al., 2013, 2009; Garreaud and Aceituno, 2007; Villalba et al.,
483 2012). This mode of variability describes the north-south movements of westerly winds and is related
484 to pressure anomalies between mid and high-latitudes in the Southern Hemisphere. In its negative
485 phase, the wind belt moves equatorward bringing cold and wet air masses to mid-latitudes of the
486 South American continent. In its positive phase, the belt moves southward, and the mid and high-
487 latitudes of South America face high pressure, warmth and low humidity. At Sainuco latitude, SAM
488 therefore exerts some control on temperature, pressure and humidity. The correlation between $\delta^{13}C$
489 at Sainuco and the SAM index are rather low, probably because $\delta^{13}C_{SAI}$ is influenced by a variety of
490 factors, including local effects. However, the spatial correlations of $\delta^{13}C_{SAI}$ with temperature at 2m
491 and high pressure on a hemispheric scale show the characteristic annular SAM pattern (Fig. 8d and

492 e). Our results are in line with those of Lavergne et al. (2017a) who found a positive and significant
493 correlation between $\delta^{13}\text{C}$ and December-February SAM.

494 At mid-latitudes, temperature variations may not only be influenced by the SAM, but also by the El
495 Niño–Southern Oscillation (ENSO) located at lower latitudes in the Pacific Ocean (Garreaud et al.,
496 2009). During normal meteorological conditions in the South Pacific, the trade winds drive the warm
497 surface waters westward. During an El Niño event, warm surface waters flow back eastward due to
498 weakening trade winds promoting higher surface water temperatures along the South American
499 coast. So, the influence of ENSO on regional climate in South America can be assessed through the
500 analysis of the correlations between proxy records and sea surface temperature (SST) in the
501 equatorial Pacific. Here, we found no significant association between $\delta^{13}\text{C}_{\text{SAI}}$ and SST indicating that
502 the influence of ENSO on climate in the study area is weak or masked by local effects.

503

504 5 Conclusions and perspectives

505

506 Variations in tree-ring width of *A. araucana* trees fit well into a broad spatial pattern of negative
507 correlations with summer temperature. Radial growth of *A. araucana* is controlled in the first order
508 by thermometric conditions in the previous year. Our results show that the carbon of the rings is
509 mostly assimilated during the current growing season, which indicates that growth is not directly
510 mediated by the accumulation of reserves. We thus hypothesize that temperature in year n-1
511 influences growth during year n by affecting the development of organs (needles, roots, etc.) where
512 growth hormones are produced.

513 $\delta^{13}\text{C}_{\text{SAI}}$ is strongly linked to several climatic parameters of the current summer. In particular, it has an
514 exceptionally strong correlation with temperature. This dependence results from the indirect effect
515 of temperature on stomatal conductance (via VPD_{max}), possibly reinforced by the effect of insolation
516 (correlated to temperature) on enzymatic activity. The strong $\delta^{13}\text{C}_{\text{SAI}}$ -temperature correlation makes

517 possible and promising the use of the cellulose $\delta^{13}\text{C}$ from *A. araucana* tree-rings at Sainuco to
518 reconstruct past temperature variations in this poorly documented area of Northern Patagonia. The
519 variations of $\delta^{13}\text{C}_{\text{SAI}}$ and summer temperature, which is under the influence of the SAM, are
520 consistent over large areas of southern South America. This pattern confirms the interest of $\delta^{13}\text{C}_{\text{SAI}}$
521 for understanding past climate on a regional scale.
522 Variations in tree-ring $\delta^{18}\text{O}_{\text{SAI}}$ appear to be controlled primarily by variations in source $\delta^{18}\text{O}$, possibly
523 because the rate of oxygen isotopic exchange between source water and sugars during cellulose
524 synthesis is high. This assumption could be reinforced by comparing the isotopic composition of the
525 *A. araucana* tree-rings with the $\delta^{18}\text{O}$ in precipitation simulated by climate models. A better
526 understanding of the causes of variation of $\delta^{18}\text{O}_{\text{SAI}}$ may thus lead to the possibility of tracing the
527 origin of air masses in relation to the modes of climate variability.

528

529 Acknowledgments:

530 Funding: This work was supported by the project THEMES from the BNP-PARIBAS foundation. T.P.
531 was supported by a 'Phare' PhD fellowship from the Commissariat à l'Énergie Atomique, France.
532 RV has been partially supported by CONICET and MINCYT (PICT 2018-03691). LAH was funded by the
533 NSF projects AGS 1903687 and AGS-1702789. We are very grateful to the two reviewers whose
534 constructive comments helped greatly to improve the manuscript.

535

536 Appendix A: Transfer functions

537

- 538 • Between $\delta^{13}\text{C}_{\text{SAI}}$ and the average value of December-January maximum temperature:

539
$$T_{\text{max DJ}} = 4.06 \delta^{13}\text{C}_{\text{SAI}} + 105.56; r^2 = 0.67 \quad \text{Eq. (A.1)}$$

- 540 • Between $\delta^{13}\text{C}_{\text{SAI}}$ and the average value of December-January maximum vapour pressure
541 deficit (VPD_{max}):

542
$$\text{VPD}_{\text{max DJ}} = 6.68 \delta^{13}\text{C}_{\text{SAI}} + 157.50; r^2 = 0.62 \quad \text{Eq. (A.2)}$$

- 543 • Between $\delta^{13}\text{C}_{\text{SAI}}$ and the average value of November-January Standardised Precipitation-
544 Evapotranspiration Index (SPEI2)

545
$$\text{SPEI2}_{\text{DJ}} = -3.75 \delta^{13}\text{C}_{\text{SAI}} - 75.77; r^2 = 0.53 \quad \text{Eq. (A.3)}$$

546

547 Figures Captions

548

549 Fig. 1: a) Location of the Sainuco site in western Argentina. b) Picture of the Sainuco site. c)
550 Umbrothermal diagram of monthly mean temperature and total precipitation data from September
551 to August between 1974 and 2014. d) Climate data from 1974 to 2014 for maximum temperature
552 (T_{max}) and vapour pressure deficit (VPD_{max}) averaged from December to January, and yearly
553 Standardised Precipitation-Evapotranspiration Index 2 (SPEI2) and precipitation (PRE, $p > 0.05$). The
554 dotted lines represent the linear trends for the data; their equations and the significance of the slope
555 (p -value) are provided.

556 Fig. 2: Sub-division of the rings into the F3/4 and L1/4 portions on a 5-mm diameter *A. araucana*
557 core. Growth direction is indicated by the white arrow and scale bar is presented on the low-right
558 corner.

559 Fig. 3: Annual variations of $\delta^{13}\text{C}$ individual series (grey), $\delta^{13}\text{C}_{\text{SAI}}$ (blue) (upper graph) and $\delta^{18}\text{O}$ series
560 (grey) and $\delta^{18}\text{O}_{\text{SAI}}$ (green) (lower graph) from 1974 to 2014. The blue and green dotted lines
561 represent the linear trends for $\delta^{13}\text{C}_{\text{SAI}}$ and $\delta^{18}\text{O}_{\text{SAI}}$.

562 Fig. 4: Upper graph, annual variations of $\delta^{13}\text{C}_{\text{SAI}}$ (solid black line) from 1974 to 2014, $\delta^{13}\text{C}_{\text{F3/4}}$ (solid
563 light grey line), $\delta^{13}\text{C}_{\text{L1/4}}$ (solid dark grey line) and $\delta^{13}\text{C}_{\text{WR}}$ (dot-dashed black line) from 1950 to 2014.
564 Lower graph, annual variations of $\delta^{18}\text{O}_{\text{SAI}}$ (solid black line) from 1974 to 2014, $\delta^{18}\text{O}_{\text{F3/4}}$ (solid dark grey

565 line), $\delta^{18}\text{O}_{\text{L1/4}}$ (solid light grey line) and $\delta^{18}\text{O}_{\text{WR}}$ (dot-dashed black line) from 1950 to 2014. The red
566 dotted lines represent the linear trends for $\delta^{13}\text{C}_{\text{SAI}}$ and $\delta^{18}\text{O}_{\text{SAI}}$.

567 Fig. 5: Sketch of the relationships based on correlation coefficients (r) among the intra-core isotopic
568 timeseries (F3/4, L1/4, lower panel), as well as between the intra-core timeseries and the isotopic
569 value for the Sainuco site chronologies ($\delta^{18}\text{O}_{\text{SAI}}$ and $\delta^{13}\text{C}_{\text{SAI}}$, upper panel). n is the current year and $n-1$
570 the previous year.

571 Fig. 6: Correlation coefficients between the $\delta^{13}\text{C}_{\text{SAI}}$ and $\delta^{18}\text{O}_{\text{SAI}}$ chronologies and regional monthly
572 maximum temperature (T_{max}), maximum vapor pressure deficit (VPD_{max}), Standardized Precipitation-
573 Evapotranspiration Index 2 (SPEI2) and Precipitation (PRE) from September of the previous growing
574 season (pSep) to April of the current growing season (Apr) from 1974 to 2014. Red dashed lines
575 represent the 99% confidence limits.

576 Fig. 7: Comparisons of temporal variations in *A. araucana* $\delta^{13}\text{C}_{\text{SAI}}$ (solid black line) at Sainuco,
577 northern Patagonia with (upper) regional mean (December-January) maximum temperature (T_{max}),
578 (middle) mean (December-January) maximum vapor pressure deficit (VPD_{max}) and (bottom) January
579 Standardized Precipitation-Evapotranspiration Index (SPEI2, calculated over December-January
580 corresponding to January) over the common interval 1974 – 2014 (41 years). To facilitate the
581 comparison with SPEI2, the $\delta^{13}\text{C}_{\text{SAI}}$ variations are shown inverted. The correlation coefficients
582 between records are also indicated.

583 Fig. 8: Field correlation maps over 1974-2014 between the $\delta^{13}\text{C}_{\text{SAI}}$ chronology (yellow dot) and a)
584 December-January T_{max} in, b) January SPEI2 c) December PRE, d) December-January T2m and e) in
585 December SLP 850 mb.

586

587 References

- 588 Arco Molina, J.G., Helle, G., Hadad, M.A., A., R.F., 2019. Variations in the intrinsic water-use efficiency
589 of north Patagonian forests under a present climate change scenario : tree age , site conditions
590 and long-term environmental effects. *Tree Physiol.* 00, 1–18.
591 <https://doi.org/10.1093/treephys/tpy144>
- 592 Barbour, M.M., Farquhar, G.D., 2004. Do pathways of water movement and leaf anatomical
593 dimensions allow development of gradients in H₂O¹⁸ between veins and the sites of
594 evaporation within leaves ? *Plant. Cell Environ.* 27, 107–121.
595 <https://doi.org/https://doi.org/10.1046/j.0016-8025.2003.01132.x>
- 596 Barbour, M.M., Walcroft, A.S., Farquhar, G.D., 2002. Seasonal variation in $\delta^{13}\text{C}$ and $\delta^{18}\text{O}$ of cellulose
597 from growth rings of *Pinus radiata*. *Plant, Cell Environ.* 25, 1483–1499.
598 <https://doi.org/10.1046/j.0016-8025.2002.00931.x>
- 599 Bariac, T., Klamecki, A., Jusserand, C., Létolle, R., 1990. Evolution de la composition isotopique de
600 l'eau (¹⁸O) dans le continuum sol-plante-atmosphère. *Geochim. Cosmochim. Acta* 54, 413–424.
601 [https://doi.org/10.1016/S0341-8162\(87\)80006-1](https://doi.org/10.1016/S0341-8162(87)80006-1)
- 602 Berry, J., Bjorkman, O., 1980. Photosynthetic Response and Adaptation to Temperature in Higher
603 Plants. *Annu. Rev. Plant Physiol.* 31, 491–543.
604 <https://doi.org/10.1146/annurev.pp.31.060180.002423>
- 605 Boninsegna, J.A., Argollo, J., Aravena, J.C., Barichivich, J., Christie, D., Ferrero, M.E., Lara, A., Le
606 Quesne, C., Luckman, B.H., Masiokas, M., Morales, M., Oliveira, J.M., Roig, F., Srur, A., Villalba,
607 R., 2009. Dendroclimatological reconstructions in South America : A review. *Palaeogeogr.*
608 *Palaeoclimatol. Palaeoecol.* 281, 210–228. <https://doi.org/10.1016/j.palaeo.2009.07.020>
- 609 Briffa, K.R., 1995. Interpreting High-Resolution Proxy Climate Data — The Example of
610 Dendroclimatology. *Anal. Clim. Var.* 77–94. https://doi.org/10.1007/978-3-662-03744-7_5
- 611 Brooks, J.R., Barnard, H.R., Coulombe, R., McDonnell, J.J., 2009. Ecohydrologic separation of water
612 between trees and streams in a Mediterranean climate. *Nat. Geosci.* 3, 100–104.

613 <https://doi.org/10.1038/ngeo722>

614 Brumos, J., Robles, L.M., Yun, J., Vu, T.C., Jackson, S., Alonso, J.M., Stepanova, A.N., 2018. Local Auxin
615 Biosynthesis Is a Key Regulator of Plant Development. *Dev. Cell* 47, 1–13.
616 <https://doi.org/10.1016/j.devcel.2018.09.022>

617 Burns, B., 1991. The regeneration dynamics of *Araucaria araucana*.

618 Burns, B.R., 1993. Fire-induced dynamics of *Araucaria araucana*-*Nothofagus antarctica* forest in the
619 southern Andes. *J. Biogeogr.* 20, 669–685. <https://doi.org/https://doi.org/10.2307/2845522>

620 Buttò, V., Deslauriers, A., Rossi, S., Rozenberg, P., Shishov, V., Morin, H., 2020. The role of plant
621 hormones in tree-ring formation. *Trees* 34, 315–335. [https://doi.org/10.1007/s00468-019-](https://doi.org/10.1007/s00468-019-01940-4)
622 [01940-4](https://doi.org/10.1007/s00468-019-01940-4)

623 Cernusak, L.A., Barbour, M.M., Arndt, S.K., Cheesman, A.W., English, N.B., Feild, T.S., Helliker, B.R.,
624 Holloway-Phillips, M.M., Holtum, J.A.M., Kahmen, A., Mcinerney, F.A., Munksgaard, N.C.,
625 Simonin, K.A., Song, X., Stuart-Williams, H., West, J.B., Farquhar, G.D., 2016. Stable isotopes in
626 leaf water of terrestrial plants. *Plant Cell Environ.* 39, 1087–1102.
627 <https://doi.org/10.1111/pce.12703>

628 Cheesman, A.W., Cernusak, L.A., 2016. Infidelity in the outback : climate signal recorded in $\Delta 18 O$ of
629 leaf but not branch cellulose of eucalypts across an Australian aridity gradient. *Tree Physiol.* 37,
630 554–564. <https://doi.org/10.1093/treephys/tpw121>

631 Coplen, T.B., 1996. New guidelines for reporting stable hydrogen, carbon, and oxygen isotope-ratio
632 data. *Geochim. Cosmochim. Acta* 60, 3359–3360. [https://doi.org/10.1016/0016-](https://doi.org/10.1016/0016-7037(96)00263-3)
633 [7037\(96\)00263-3](https://doi.org/10.1016/0016-7037(96)00263-3)

634 Cuny, H.E., Rathgeber, C.B.K., 2014. Une synthèse sur le fonctionnement et la régulation des
635 processus cellulaires de la formation du bois. *Rev. For. Fr.* 66, 761–777.
636 <https://doi.org/10.4267/2042/56750>

637 Davies, W.K.D., 2010. The Plant Hormones: Their Nature, Occurrence, and Functions. *Plant*
638 *hormones*. Springer Netherlands, Dordr. 112, 1–15. <https://doi.org/10.1007/978-94-017-9655->

639 2_1

- 640 Dawson, T.E., Ehleringer, J.R., 1993. Isotopic enrichment of water in the “ woody ” tissues of plants :
641 Implications for plant water source , water uptake , and other studies which use the stable
642 isotopic composition of cellulose. *Geochim. Cosmochim. Acta* 57, 3487–3492.
643 [https://doi.org/10.1016/0016-7037\(93\)90554-A](https://doi.org/10.1016/0016-7037(93)90554-A)
- 644 del Valle, H.F., 1998. Patagonian soils: A regional synthesis. *Ecol. Austral* 8, 103–123.
- 645 Díaz-Vaz, J.E., 1984. *Araucaria Araucana*. Descripción Anatómica. *BOSQUE* 5, 117–118.
- 646 Dickmann, D.I., Kozlowski, T.T., 1970. Vegetative Reproductive Mobilization and Incorporation of
647 Photoassimilated ¹⁴C by Growing Vegetative and Reproductive Tissues of Adult *Pinus resinosa*
648 Ait. Trees. *Plant Physiol.* 45, 284–288.
- 649 Dombrosky, J., 2020. A ~1000-year ¹³C Suess correction model for the study of past ecosystems. *The*
650 *Holocene* 30, 474–478. <https://doi.org/10.1177/0959683619887416>
- 651 Dünser, K., Kleine-Vehn, J., 2015. Differential growth regulation in plants-the acid growth balloon
652 theory. *Curr. Opin. Plant Biol.* 28, 55–59. <https://doi.org/10.1016/j.pbi.2015.08.009>
- 653 Falcon-Lang, H.J., 2000. The relationship between leaf longevity and growth ring markedness in
654 modern conifer woods and its implications for palaeoclimatic studies. *Palaeogeogr.*
655 *Palaeoclimatol. Palaeoecol.* 160, 317–328. [https://doi.org/10.1016/S0031-0182\(00\)00079-1](https://doi.org/10.1016/S0031-0182(00)00079-1)
- 656 Fu, P.L., Griebinger, J., Gebrekirstos, A., Fan, Z.X., Bräuning, A., 2017. Earlywood and latewood stable
657 carbon and oxygen isotope variations in two pine species in Southwestern China during the
658 recent decades. *Front. Plant Sci.* 7, 1–12. <https://doi.org/10.3389/fpls.2016.02050>
- 659 Garreaud, R.D., Aceituno, P., 2007. *Atmospheric Circulation and Climatic Variability*. Oxford Univ.
660 Press 45–59. <https://doi.org/10.1093/oso/9780195313413.003.0010>
- 661 Garreaud, R.D., Lopez, P., Minvielle, M., Rojas, M., 2013. Large-Scale Control on the Patagonian
662 Climate. *J. Clim.* 26, 215–231. <https://doi.org/10.1175/JCLI-D-12-00001.1>
- 663 Garreaud, R.D., Vuille, M., Compagnucci, R., Marengo, J., 2009. Present-day South American climate.
664 *Palaeogeogr. Palaeoclimatol. Palaeoecol.* 281, 180–195.

665 <https://doi.org/10.1016/j.palaeo.2007.10.032>

666 Glerum, C., 1980. Food sinks and food reserves of trees in temperate climates. *New Zeal. J. For. Sci.*
667 10, 176–185.

668 Gonfiantini, R., Gratziu, S., Tongiorgi, E., 1965. Oxygen Isotopic Composition of Water in Leaves. *Isot.*
669 *Radiat. Soil-Plant Nutr. Stud.* 405–410.

670 Grießinger, J., Langhamer, L., Schneider, C., Saß, B. -I., Steger, D., Skvarca, P., Braun, M.H., Meier,
671 W.J.-H., Srur, A.M., Hochreuther, P., 2018. Imprints of Climate Signals in a 204 Year $\delta^{18}\text{O}$ Tree-
672 Ring Record of *Nothofagus pumilio* From Perito Moreno Glacier , Southern Patagonia (50°S).
673 *Front. Earth Sci.* 6, 1–17. <https://doi.org/10.3389/feart.2018.00027>

674 Grossiord, C., Buckley, T.N., Cernusak, L.A., Novick, K.A., Poulter, B., Siegwolf, R.T.W., Sperry, J.S.,
675 Mcdowell, N.G., 2020. Tansley review Plant responses to rising vapor pressure deficit. *New*
676 *Phytol.* 226, 1550–1566. <https://doi.org/10.1111/nph.16485>

677 Hadad, M.A., González-Reyes, Á., Roig, F.A., Matskovsky, V., Cherubini, P., 2021. Tree-ring-based
678 hydroclimatic reconstruction for the northwest Argentine Patagonia since 1055 CE and its
679 teleconnection to large-scale atmospheric circulation. *Glob. Planet. Change* 202.
680 <https://doi.org/10.1016/j.gloplacha.2021.103496>

681 Hadad, M.A., Roig, F.A., 2016. Sex-related climate sensitivity of *Araucaria araucana* Patagonian
682 forest-steppe ecotone. *For. Ecol. Manage.* 362, 130–141.
683 <https://doi.org/10.1016/j.foreco.2015.11.049>

684 Hadad, M.A., Roig, F.A., Boninsegna, J.A., Patón, D., 2014. Age effects on the climatic signal in
685 *Araucaria araucana* from xeric sites in Patagonia, Argentina. *Plant Ecol. Divers.* 1–9.
686 <https://doi.org/10.1080/17550874.2014.980350>

687 Harris, I., Osborn, T.J., Jones, P., Lister, D., 2020. Version 4 of the CRU TS monthly high-resolution
688 gridded multivariate climate dataset. *Sci. Data* 7, 1–18. [https://doi.org/10.1038/s41597-020-](https://doi.org/10.1038/s41597-020-0453-3)
689 0453-3

690 Helle, G., Schleser, G.H., 2004. Beyond CO₂-fixation by Rubisco - An interpretation of $^{13}\text{C}/^{12}\text{C}$

691 variations in tree rings from novel intra-seasonal studies on broad-leaf trees. *Plant, Cell Environ.*
692 27, 367–380. <https://doi.org/10.1111/j.0016-8025.2003.01159.x>

693 Hersbach, H., Bell, B., Berrisford, P., Hirahara, S., Horányi, A., Muñoz-Sabater, J., Nicolas, J., Peubey,
694 C., Radu, R., Schepers, D., Simmons, A., Soci, C., Abdalla, S., Abellan, X., Balsamo, G., Bechtold,
695 P., Biavati, G., Bidlot, J., Bonavita, M., De Chiara, G., Dahlgren, P., Dee, D., Diamantakis, M.,
696 Dragani, R., Flemming, J., Forbes, R., Fuentes, M., Geer, A., Haimberger, L., Healy, S., Hogan,
697 R.J., Hólm, E., Janisková, M., Keeley, S., Laloyaux, P., Lopez, P., Lupu, C., Radnoti, G., de Rosnay,
698 P., Rozum, I., Vamborg, F., Villaume, S., Thépaut, J.N., 2020. The ERA5 global reanalysis. *Q. J. R.*
699 *Meteorol. Soc.* 146, 1999–2049. <https://doi.org/10.1002/qj.3803>

700 Holmes, R., 1983. Computer-Assisted Quality Control in Tree-Ring Dating and Measurement. *Tree-*
701 *ring Bull.* 43, 69–78.

702 Kagawa, A., Sugimoto, A., Maximov, T.C., 2006. Seasonal course of translocation, storage and
703 remobilization of ¹³C pulse-labeled photoassimilate in naturally growing *Larix gmelinii* saplings.
704 *New Phytol.* 171, 793–804. <https://doi.org/10.1111/j.1469-8137.2006.01780.x>

705 Kimak, A., Leuenberger, M., 2015. Are carbohydrate storage strategies of trees traceable by early–
706 latewood carbon isotope differences? *Trees* 29, 859–870. <https://doi.org/10.1007/s00468-015->
707 1167-6

708 Knöller, K., Boettger, T., Weise, S.M., Gehre, M., 2005. Carbon isotope analyses of cellulose using two
709 different on-line techniques (elemental analysis and high-temperature pyrolysis) - A
710 comparison. *Rapid Commun. Mass Spectrom.* 19, 343–348. <https://doi.org/10.1002/rcm.1793>

711 Kozłowski, T.T., 1992. Carbohydrate sources and sinks in woody plants. *Bot. Rev.* 58, 107–222.
712 <https://doi.org/10.1007/BF02858600>

713 Kress, A., Young, G.H.F., Saurer, M., Loader, N.J., Siegwolf, R.T.W., McCarroll, D., 2009. Stable isotope
714 coherence in the earlywood and latewood of tree-line conifers. *Chem. Geol.* 268, 52–57.
715 <https://doi.org/10.1016/j.chemgeo.2009.07.008>

716 Lara, A., Villalba, R., Urrutia-Jalabert, R., González-Reyes, A., Aravena, J.C., Luckman, B.H., Cuq, E.,

717 Rodríguez, C., Wolodarsky-Franke, A., 2020. +A 5680-year tree-ring temperature record for
718 southern South America. *Quat. Sci. Rev.* 228, 1–14.
719 <https://doi.org/10.1016/j.quascirev.2019.106087>

720 Lavergne, A., 2016. Evaluation of tree-ring archive as paleoclimatic tracer in northern Patagonia.
721 Lavergne, A., Daux, V., Pierre, M., Stievenard, M., Srur, A., Villalba, R., 2018. Past Summer
722 Temperatures Inferred From Dendrochronological Records of *Fitzroya cupressoides* on the
723 Eastern Slope of the Northern Patagonian Andes. *J. Geophys. Res. Biogeosciences*.
724 <https://doi.org/10.1002/2017JG003989>

725 Lavergne, A., Gennaretti, F., Risi, C., Daux, V., Boucher, E., Savard, M.M., Naulier, M., Villalba, R.,
726 Bégin, C., Guiot, J., 2017b. Modelling tree ring cellulose $\delta^{18}\text{O}$ variations in two temperature-
727 sensitive tree species from North and South America. *Clim. Past* 13, 1515–1526.
728 <https://doi.org/https://doi.org/10.5194/cp-13-1515-2017>

729 Lavergne, A., Daux, V., Villalba, R., Pierre, M., Stievenard, M., Srur, A.M., 2017a. Improvement of
730 isotope-based climate reconstructions in Patagonia through a better understanding of climate
731 influences on isotopic fractionation in tree rings. *Earth Planet. Sci. Lett.* 1, 1–9.
732 <https://doi.org/10.1016/j.epsl.2016.11.045>

733 Lavergne, A., Daux, V., Villalba, R., Pierre, M., Stievenard, M., Srur, A.M., Vimeux, F., 2016. Are the
734 $\delta^{18}\text{O}$ of *F. cupressoides* and *N. pumilio* promising proxies for climate reconstructions in
735 northern Patagonia? *J. Geophys. Res. Biogeosciences* 121, 767–776.
736 <https://doi.org/10.1002/2015JG003260>

737 Le Quesne, C., Stahle, D.W., Cleaveland, M.K., Therrell, M.D., Aravena, J.C., Barichivich, J., 2006.
738 Ancient *Austrocedrus* tree-ring chronologies used to reconstruct central Chile precipitation
739 variability from A.D. 1200 to 2000. *J. Clim.* 19, 5731–5744. <https://doi.org/10.1175/JCLI3935.1>

740 Leavitt, S.W., Danzer, S.R., 1993. Method for Batch Processing Small Wood Samples to Holocellulose
741 for Stable-Carbon Isotope Analysis. *Anal. Chem.* 65, 87–89.
742 <https://doi.org/https://doi.org/10.1021/ac00049a017>

743 Ljung, K., Hull, A.K., Celenza, J., Yamada, M., Estelle, M., Normanly, J., Sandberg, G., 2005. Sites and
744 regulation of auxin biosynthesis in arabidopsis roots. *Plant Cell* 17, 1090–1104.
745 <https://doi.org/10.1105/tpc.104.029272>

746 Majda, M., Robert, S., 2018. The role of auxin in cell wall expansion. *Int. J. Mol. Sci.* 19, 1–21.
747 <https://doi.org/10.3390/ijms19040951>

748 Meier, W.J., 2019. Past and recent climate variability and glacier fluctuations across the Southern
749 Patagonian Andes.

750 Morales, M.S., Christie, D.A., Villalba, R., Argollo, J., Pacajes, J., Silva, J.S., Alvarez, C.A., Llancabure,
751 J.C., Gamboa, C.C.S., 2012. Precipitation changes in the South American Altiplano since 1300 AD
752 reconstructed by tree-rings. *Clim. Past* 8, 653–666. <https://doi.org/10.5194/cp-8-653-2012>

753 Mott, K.A., Woodrow, I.E., 2000. Modelling the role of Rubisco activase in limiting non-steady-state
754 photosynthesis. *J. Exp. Bot.* 51, 399–406. https://doi.org/10.1093/jexbot/51.suppl_1.399

755 Mundo, I.A., Jun, F.A.R., Villalba, R., Kitzberger, T., Barrera, M.D., 2012. *Araucaria araucana* tree-ring
756 chronologies in Argentina : spatial growth variations and climate influences. *Trees* 26, 443–458.
757 <https://doi.org/10.1007/s00468-011-0605-3>

758 Muñoz, A.A., Barichivich, J., Christie, A.D., Dorigo, W., Sauchyn, D., Gonzalez-Reyes, A., Villalba, R.,
759 Lara, A., Riquelme, N., Gonzalez, M.E., 2013. Patterns and drivers of *Araucaria araucana* forest
760 growth along a biophysical gradient in the northern Patagonian Andes : Linking tree rings with s.
761 *Austral Ecol.* 12pp. <https://doi.org/10.1111/aec.12054>

762 Puchi, P.F., Camarero, J.J., Battipaglia, G., Carrer, M., 2021. Retrospective analysis of wood
763 anatomical traits and tree-ring isotopes suggests site-specific mechanisms triggering *Araucaria*
764 *araucana* drought-induced dieback. *Glob. Chang. Biol.* 27, 6394–6408.
765 <https://doi.org/10.1111/gcb.15881>

766 Rathgeber, C.B.K., 2020. *Ecophysiology of Tree-ring Formation : Concepts, Methods and Applications.*

767 Rathgeber, C.B.K., Cuny, H.E., Fonti, P., 2016. Biological basis of tree-ring formation: A crash course.
768 *Front. Plant Sci.* 7, 1–7. <https://doi.org/10.3389/fpls.2016.00734>

769 Requena-Rojas, E.J., Morales, M., Villalba, R., 2020. Dendroclimatological assessment of *Polylepis*
770 *rodolfo-vasquezii*: A novel *Polylepis* species in the Peru highlands. *Dendrochronologia* 62,
771 125722. <https://doi.org/10.1016/j.dendro.2020.125722>

772 Roden, J.S., Farquhar, G.D., 2012. A controlled test of the dual-isotope approach for the
773 interpretation of stable carbon and oxygen isotope ratio variation in tree rings. *Tree Physiol.* 32,
774 490–503. <https://doi.org/10.1093/treephys/tps019>

775 Rodriguez-Caton, M., Andreu-Hayles, L., Morales, M.S., Daux, V., Christie, D.A., Coopman, R.E.,
776 Alvarez, C., Rao, M.P., Aliste, D., Flores, F., Villalba, R., 2021. Different climate sensitivity for
777 radial growth, but uniform for tree-ring stable isotopes along an aridity gradient in *Polylepis*
778 *tarapacana*, the world’s highest elevation tree-species . *Tree Physiol.*
779 <https://doi.org/10.1093/treephys/tpab021>

780 Roig, F.A., Siegwolf, R., Boninsegna, J.A., 2006. Stable oxygen isotopes ($\delta^{18}O$) in *Austrocedrus*
781 *chilensis* tree rings reflect climate variability in northwestern Patagonia , Argentina. *Int. J.*
782 *Biometeorol.* 51, 97–105. <https://doi.org/10.1007/s00484-006-0049-4>

783 Rothfuss, Y., Javaux, M., 2017. Reviews and syntheses : Isotopic approaches to quantify root water
784 uptake : a review and comparison of methods. *Biogeosciences* 14, 2199–2224.
785 <https://doi.org/10.5194/bg-14-2199-2017>

786 Running, S.W., 1976. Environmental control of leaf water conductance in conifers. *Can. J. For. Res.* 6,
787 104–112. <https://doi.org/https://doi.org/10.1139/x76-013>

788 Scheidegger, Y., Saurer, M., Bahn, M., Siegwolf, R., 2000. Linking stable oxygen and carbon isotopes
789 with stomatal conductance and photosynthetic capacity: A conceptual model. *Oecologia* 125,
790 350–357. <https://doi.org/10.1007/s004420000466>

791 Scheuring, D., Löffke, C., Krüger, F., Kittelmann, M., Eisa, A., Hughes, L., Smith, R.S., Hawes, C.,
792 Schumacher, K., Kleine-Vehn, J., 2016. Actin-dependent vacuolar occupancy of the cell
793 determines auxin-induced growth repression. *Proc. Natl. Acad. Sci. U. S. A.* 113, 452–457.
794 <https://doi.org/10.1073/pnas.1517445113>

795 Sprenger, M., Leistert, H., Gimbel, K., Weiler, M., 2016. Illuminating hydrological processes at the
796 soil-vegetation- atmosphere interface with water stable isotopes. *Rev. Geophys.* 54, 674–704.
797 <https://doi.org/10.1002/2015RG000515>

798 Stokes, M.A., Smiley, T.L., 1968. *An Introduction to Tree-Ring Dating*.

799 Szejner, P., Clute, T., Anderson, E., Evans, M.N., Hu, J., 2020. Reduction in lumen area is associated
800 with the $\delta^{18}\text{O}$ exchange between sugars and source water during cellulose synthesis. *New*
801 *Phytol.* 226, 1583–1593. <https://doi.org/10.1111/nph.16484>

802 Taiz, L., Zeiger, E., 2002. *Plant physiology (Third Edition)*, Science progress. Sinauer Associates, Inc.,
803 Publishers, Sunderland. <https://doi.org/10.1017/9781108486392>

804 Teten, O., 1930. Über einige meteorologische Begriffe. *Zeitschrift für Geophys.* 6, 297–309.

805 Tognetti, R., Lombardi, F., Lasserre, B., Cherubini, P., Marchetti, M., 2014. Tree-Ring Stable Isotopes
806 Reveal Twentieth-Century Increases in Water-Use Efficiency of *Fagus sylvatica* and *Nothofagus*
807 spp. in Italian and Chilean Mountains. *PLoS One* 9, 1–16.
808 <https://doi.org/10.1371/journal.pone.0113136>

809 Tortorelli, L.A., 1956. *Maderas y bosques argentinos*. Editorial Acme, Buenos Aires.

810 Urrutia-Jalabert, R., Malhi, Y., Barichivich, J., Lara, A., Delgado-Huertas, A., Rodríguez, C.G., Cuq, E.,
811 2015c. Increased water use efficiency but contrasting tree growth patterns in Fitzroya
812 cupressoides forests of southern Chile during recent decades. *J. Geophys. Res. Biogeosciences*
813 120, 2505–2524. <https://doi.org/10.1002/2015JG003098>

814 Veblen, T.T., 1982. Regeneration Patterns in *Araucaria araucana* Forests in Chile. *J. Biogeogr.* 9, 11.
815 <https://doi.org/10.2307/2844727>

816 Veblen, T.T., Burns, B.R., Kitzberger, T., Lara, A., Villalba, R., 1995. *The Ecology of the Conifers of*
817 *Southern South America*. *Ecol. South. Conifers* 120–155.

818 Vicente-Serrano, S.M., Beguería, S., López-Moreno, J.I., 2010. A multiscalar drought index sensitive to
819 global warming: The standardized precipitation evapotranspiration index. *J. Clim.* 23, 1696–
820 1718. <https://doi.org/10.1175/2009JCLI2909.1>

821 Villalba, R., 1995. Geographical variations in tree-growth responses to climate in the Southern Andes.
822 Cambios cuaternarios en América del Sur 307–317.

823 Villalba, R., 1990. Climatic Fluctuations in Northern Patagonia during the Last 1000 Records Years as
824 Inferred from Tree-Ring Records. *Quat. Res.* 34, 346–360.

825 Villalba, R., Lara, A., Masiokas, M.H., Urrutia, R., Luckman, B.H., Marshall, G.J., Mundo, I.A., Christie,
826 D.A., Cook, E.R., Neukom, R., Allen, K., Fenwick, P., Boninsegna, J.A., Srur, A.M., Morales, M.S.,
827 Araneo, D., Palmer, J.G., Cuq, E., Aravena, J.C., Holz, A., LeQuesne, C., 2012. Unusual Southern
828 Hemisphere tree growth patterns induced by changes in the Southern Annular Mode. *Nat.*
829 *Geosci.* 5, 793–798. <https://doi.org/10.1038/ngeo1613>

830 Villalba, R., Lara, A., Boninsegna, J.A., Masiokas, M., Delgado, S., Aravena, J.C., Roig, F.A., Schmelter,
831 A., Wolodarsky-Franke, A., Ripalta, A., 2003. Large-Scale Temperature Changes across the
832 Southern Andes: 20th Century Variations in the Context of the Past 400 Years. *Clim. Change* 97,
833 131–141. <https://doi.org/10.1023/A>

834 Villalba, R., Cook, E.R., Jacoby, G.C., D'Arrigo, R.D., Veblen, T.T., Jones, P.D., 1998. Tree-ring based
835 reconstructions of northern Patagonia precipitation since AD 1600. *The Holocene* 8, 659–674.
836 <https://doi.org/10.1191/095968398669095576>

837 Villalba, R., Boninsegna, J.A., Lara, A., Veblen, T.T., Roig, F.A., Aravena, J.C., Ripalta, A., 1996.
838 Interdecadal climatic variations in millennial temperature reconstructions from southern South
839 America. Jones, P.D., Bradley, R.S., Jouzel, J. (Eds.), *Clim. Var. Forcing Mech. Last 2000 years*
840 *NATO ASI Ser.* 141, 161–189. <https://doi.org/10.1007/978-3-642-61113-1>

841 Wigley, T.M.L., Briffa, K.R., Jones, P.D., 1984. On the average value of correlated time series, with
842 applications in dendroclimatology and hydrometeorology. *J. Clim. Appl. Meteorol.* 23, 201–213.
843 [https://doi.org/http://dx.doi.org/10.1175/1520-0450\(1984\)023<0201:OTAVOC>2.0.CO;2](https://doi.org/http://dx.doi.org/10.1175/1520-0450(1984)023<0201:OTAVOC>2.0.CO;2)

844 Woodley, E.J., Loader, N.J., McCarroll, D., Young, G.H.F., Robertson, I., Heaton, T.H.E., Gagen, M.H.,
845 Warham, J.O., 2012. High-temperature pyrolysis/gas chromatography/isotope ratio mass
846 spectrometry: Simultaneous measurement of the stable isotopes of oxygen and carbon in

847 cellulose. *Rapid Commun. Mass Spectrom.* 26, 109–114. <https://doi.org/10.1002/rcm.5302>

848 Yamaguchi, D.K., 1991. A simple method for cross-dating increment cores from living trees. *Can. J.*
849 *For. Res.* 414–416.

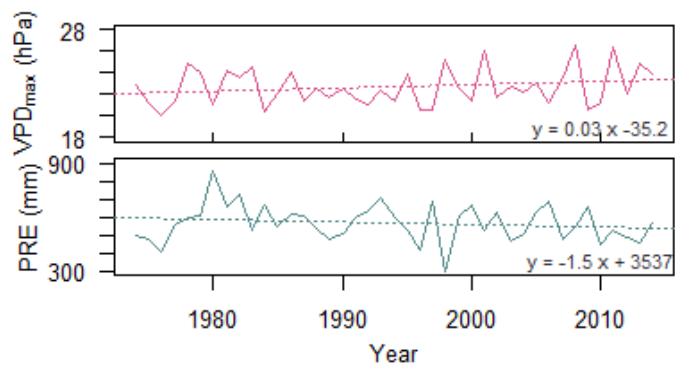
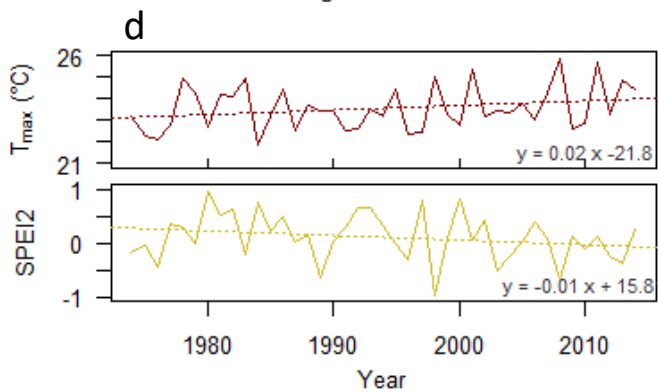
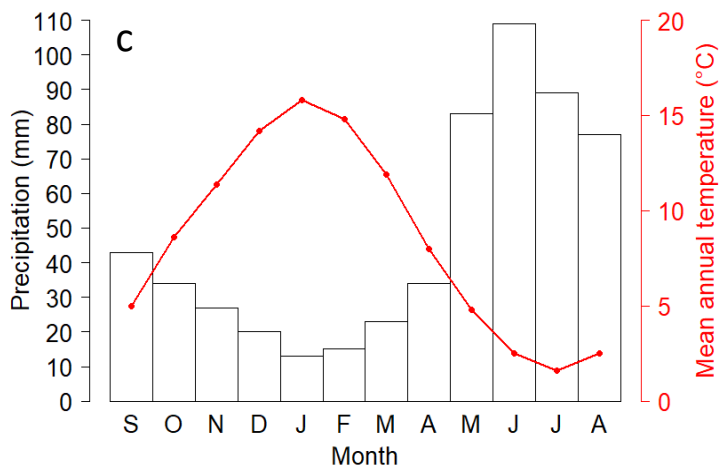
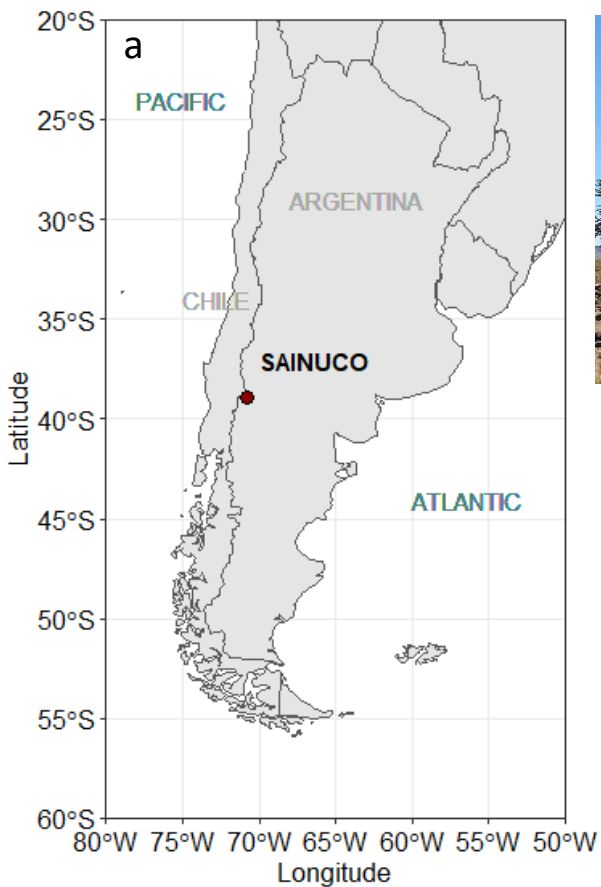
850 Zhao, Y., 2010. Auxin biosynthesis and its role in plant development. *Annu. Rev. Plant Biol.* 61, 49–64.
851 <https://doi.org/10.1146/annurev-arplant-042809-112308>

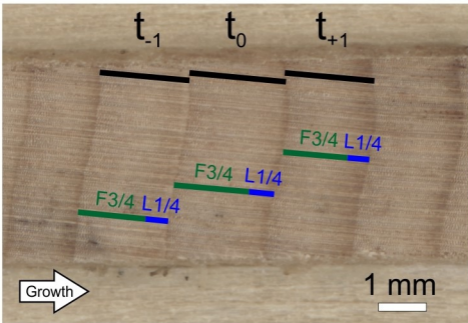
852 Zhong, R., Ye, Z.-H., 2009. Secondary Cell Walls. *Encycl. Life Sci.*
853 <https://doi.org/10.1002/9780470015902.a0021256>

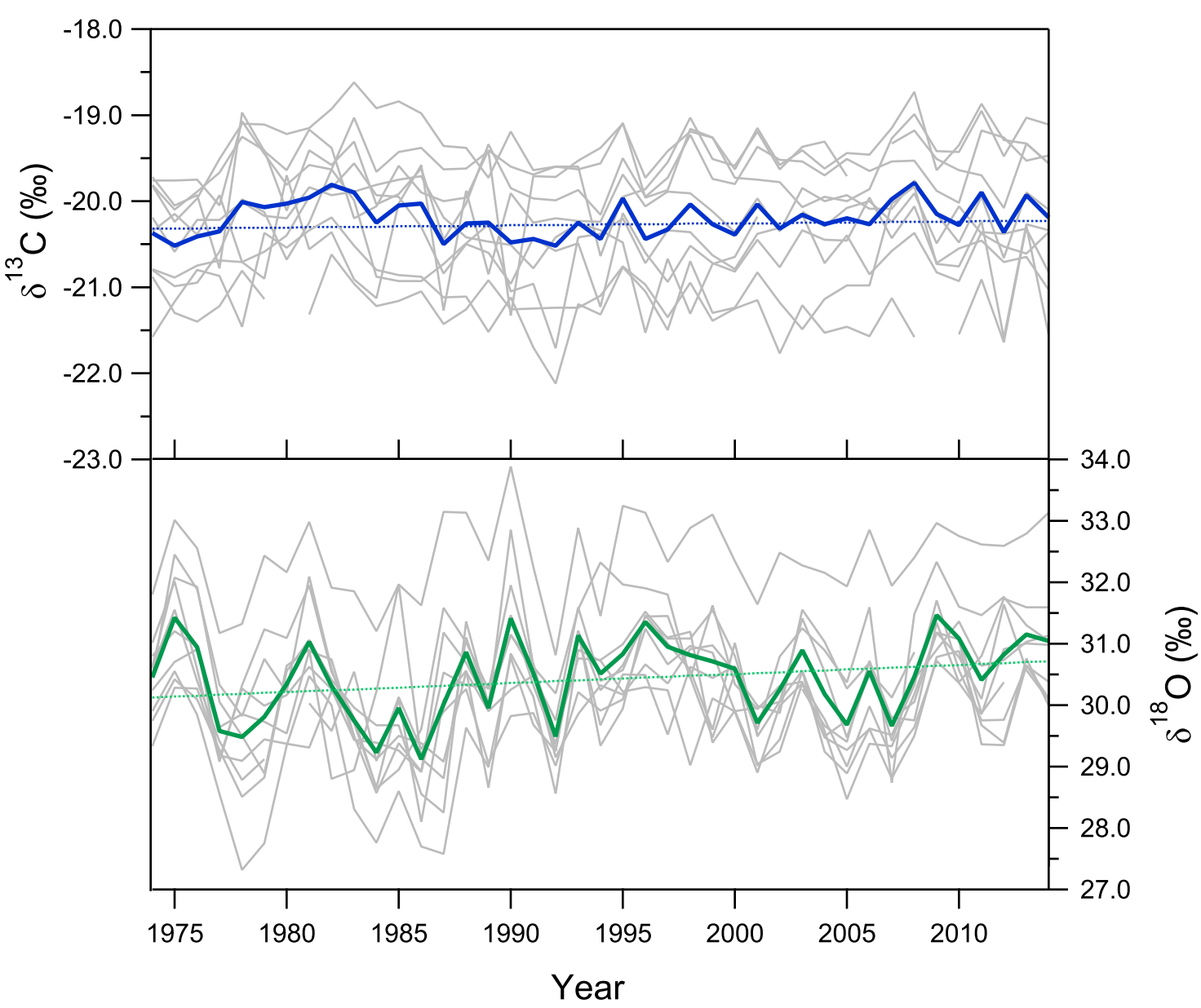
854 Zweifel, R., Sterck, F., 2018. A Conceptual Tree Model Explaining Legacy Effects on Stem Growth.
855 *Front. For. Glob. Chang.* 1, 1–9. <https://doi.org/10.3389/ffgc.2018.00009>

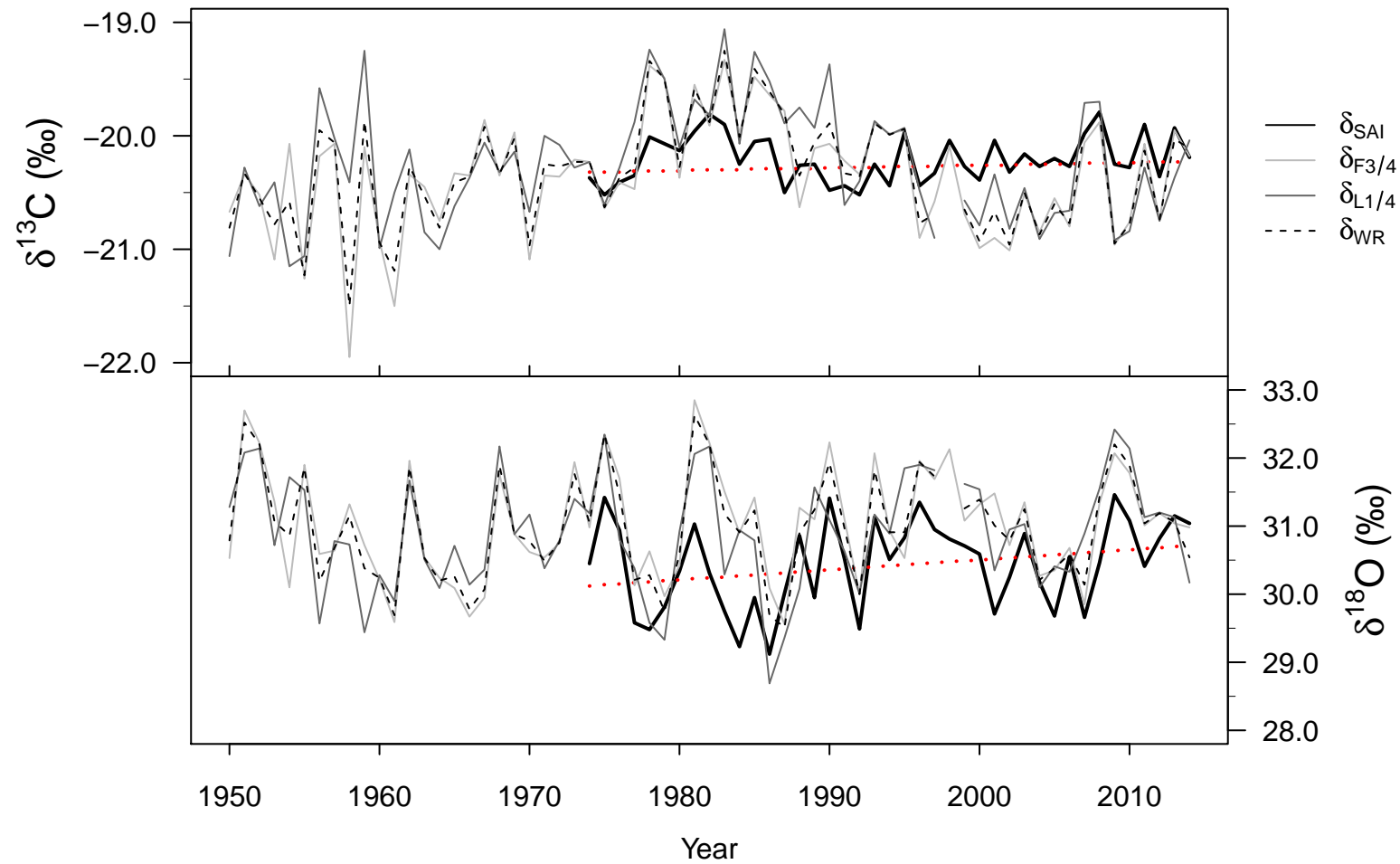
856

857







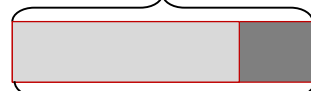
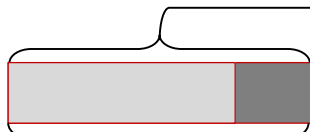


Carbon

Oxygen

-0.23

SAI



0.52

0.71

Intra-core



0.51

0.46

0.68


0.65


0.34

0.71


0.51

0.70


 : One ring

 : F3/4

 : Correlation inter-core

 : Current year

 : L1/4

 : Correlation intra-core

